Polarization properties and oxygen-vacancy distribution of $SrBi_2Ta_2O_9$ ceramics modified by Ce and Pr

Masaru Miyayama, and Yuji Noguchi
Institute of Industrial Science, The University of Tokyo
4-6-1 Komaba, Meguro-ku, Tokyo 153-8505, Japan

ABSTRACT

Effects of cerium and praseodymium modifications on the ferroelectric distortion, defect structure, and polarization properties were investigated for layered ferroelectric $SrBi_2Ta_2O_9$ (SBT). Neutron powder diffraction and x-ray photoelectron analyses showed that these rare-earth ions (RE) are substituted at the Sr site as RE^{3+} and that Sr vacancies are created for compensating the charge difference between Sr^{2+} and RE^{3+}. Oxygen vacancies were present in perovskite layers for Pr-SBT, but in both perovskite and Bi_2O_2 layers for Ce-SBT. Polarization measurements using dense ceramics indicated that Pr modification led to an marked improvement of polarization properties while Ce-modified SBT exhibited a lower remanent polarization caused by domain pinning and polarization-hysteresis shift. The oxygen vacancies in the Bi_2O_2 layers are suggested to induce the deterioration such as the domain pinning and hysteresis shift in the SBT system.

KEYWORDS: Defects, Dielectric properties, Ferroelectric properties, Neutron powder diffraction

INTRODUCTION

Ferroelectric thin films have been intensively studied for use in non-volatile random access memory (NvRAM). Ferroelectric $SrBi_2Ta_2O_9$ (SBT) has played a key role in the ferroelectric materials with high durability against a repeated switching of polarization states. [1,2] In the crystal structure of SBT, perovskite layers, $SrTa_2O_7$, composed of double TaO_6 octahedra with Sr at the *A* site, are interleaved with Bi_2O_2 layers. The Bi_2O_2 layers act as insulating paraelectric layers and largely control the electronic response (electrical conductivity, band gap, etc,), [3] while the ferroelectricity arises in the perovskite layers.[4-6] It is argued that the Bi_2O_2 layers perform the primary function of preventing degradation of the remanent charge. [1] The ferroelectricity is attributed to the rotation and tilting of TaO_6 octahedra as well as the off-center displacement of Ta ions in the octahedra.[6] Recently, Noguchi *et al.* [6-8] have reported that Sr vacancies as well as oxygen vacancies strongly affect polarization properties. In spite of its technological importance, however, the understanding of the defect structure is SBT is far from complete because of the complexity of its layered structure.

In this study, the ferroelectric distortion and defect structure of Ce- and Pr-modified SBTs were investigated through a high-resolution neutron diffraction combined with Rietveld analysis, and the polarization properties measured using dense ceramics were discussed in view of structure distortion defect structure. It is suggested that oxygen vacancies in the Bi_2O_2 layers play a crucial role in the polarization properties in the SBT system.

EXPERIMENT

Ceramic samples of SBT, $RE_{2x/3}Sr_{1-x}Bi_2Ta_2O_9$ (RE-SBT, RE=Ce, Pr : x=0.2) were prepared by a solid-state reaction. Raw materials of CeO_2, Pr_6O_{11}, $SrCO_3$, Bi_2O_3, and Ta_2O_5 of 99.99 % purity were thoroughly mixed and calcined at 1100□ for 4 h for powder diffraction measurements. To obtain dense samples for electrical measurements, excess Bi_2O_3 of 2 at.% of the stoichiometric composition was added to the starting powder. Uniaxially pressed pellets using the powder calcined at 1100□ for 4 h were subjected to a cold isostatic press (CIP) treatment at 300 MPa, and then sintered at 1250□ for 1-2 h. This excess-Bi_2O_3 addition led to a high relative density of over 95%. The sintered pellets were polished into thin sheets of 0.1-0.3 mm thickness for polarization and dielectric measurements. The X-ray diffraction (XRD) measurements on the polished surface of the dense samples revealed there was no preferred orientation.

Time-of-flight neutron powder diffraction data were collected at 25□ using the Vega diffractometer at KENS[9]. Structural parameters were refined by the Rietveld method using the program RIETAN-TN[10] based on $A2_1am$ orthorhombic symmetry. In the structure analysis, we carefully examined the occupancies of oxide ions in crystals. The first analysis was conducted under the condition that all sites were occupied by oxide ions (occupation=1.0). Then, occupancy parameters of oxide ions were refined in the condition that thermal parameters (B_{eq}) were fixed at the values in the last analysis when oxygen vacancies were not considered. Finally, the occupancy parameters of oxide ions were refined simultaneously with the B_{eq}.

We measured X-ray photoelectron spectroscopy (XPS) using a Quantum-2000 (ULVAC-PHI) spectrometer (Al $K\alpha$ x-ray source). The XPS measurements were conducted on the clean surface of the fractured ceramics, the spectra were obtained without any disturbance of surface caused by a sputter beam and so on. The binding energy scale was calibrated using the C1*s* line that appears in the spectra due to the usual carbon contamination.

Results and discussion

It has been demonstrated that Bi and Rear-earth elements (La and Nd etc.) are substituted at the *A* site as trivalent ions and that the charge neutrality is satisfied through the formation of Sr vacancies (V**Erreur!**).[5-8] Neutron powder diffraction data of Ce- and Pr-SBT (x=0.2) were analyzed by the Rietveld method in the same manner, and the results are indicated in Fig. 1. The calculated pattern assuming that these RE ions occupy the *A* site with Sr vacancies fitted fairly well to the observed data, and any impurity peak did not detected. The final *R* factors and lattice parameters are listed in Table I. The detailed structural parameters of Ce- and Pr-SBTs are summarized in Table II and III, respectively. The crystal structure and the detailed sites are depicted in Fig. 2.

Figure 3 shows the lattice parameters and volume of RE-SBT (x=0.2) as a function of ionic radius of RE^{3+} at the 12-coordinated site. Since we could not find the ionic radius of Ce^{3+}, the ionic radius is assumed to be the average of those of La^{3+} and Pr^{3+} for convenience. La-SBT showed almost the same lattice volume as Ce-SBT, however the polarization properties were quite different, as described below. For the samples of Pr-, Nd-, and Sm-SBTs, the lattice volume (V) decreased with decreasing ionic radius. Except for Sm-SBT having a longer a than b, the parameter b was larger than a (the polar axis). Furthermore, the relation between lattice parameters and Nd content (x) was examined.[7] With increasing Nd content (x), lattice volume and parameter c monotonically decreased due to its smaller ionic radius of Nd^{3+} than Sr^{2+}.

XPS measurements were performed for several RE-SBTs. For Pr-SBT, the spectra of Pr-SBT(x=0.2) powder, and those of Pr_2O_3 and Pr_6O_{11} powders were carefully examined.[11,12] For Pr_2O_3, the peak attributed to Pr^{3+} appeared at around 935 eV and 955 eV. In the spectrum of Pr_6O_{11} that contains both of Pr^{3+} and Pr^{4+} (the molar ratio of Pr^{3+} to Pr^{4+} is 2 to 1), the apparent peaks originating in Pr^{4+} were detected at the lower binding energy of Pr^{3+} peaks. For Pr-SBT, only the Pr^{3+} peaks were detected but Pr^{4+} was not present.[11] The results of neutron diffraction and XPS analyses lead to the conclusion that RE cations are substituted at the *A* site with trivalent cations and that the formation of V**Erreur!** compensates the charge deference between Sr^{2+} and RE^{3+}. The substitution of RE at the *A* site is expressed by the formula;

$$RE_2O_3 \rightarrow 2RE\textbf{Erreur!} + 3O\textbf{Erreur!} + V\textbf{Erreur!}, \quad (1)$$

where RE**Erreur!** indicates RE^{3+} at the Sr^{2+} site (*A* site), and O**Erreur!** denotes O^{2-} at the oxygen site.

The detailed structural analysis revealed the presence of oxygen vacancies (V**Erreur!**) as well as V**Erreur!** in Ce- and Pr-SBTs (see Tables II and III). The occupancy at the O1 site was about 0.96-0.97 for both samples, which was lower than the other sites. A significant difference between Ce- and Pr-SBTs was found on V**Erreur!** at the O3 site in the Bi_2O_2 layers. While Ce-SBT had about 1.7% vacancies, Pr-SBT had no vacancies at the O3 site in the Bi_2O_2 layers. It has been reported for SBT thin films that oxygen vacancies are preferentially present near the Bi ions in the Bi_2O_2 layers.[13] The relation between the V**Erreur!** distribution and polarization properties will be discussed later.

Figure 4 indicates the temperature dependence of dielectric permittivity at a frequency of 10 kHz, 100kHz, and 1 MHz. While Ce-SBT did not show a frequency dependence of dielectric permittivity (as observed in SBT[7]), Pr-SBT showed a frequency dispersion of permittivity. The Curie temperature (T_C) estimated from the peak temperature of SBT was 295□. [7] The substitution of Ce did not affect T_C, while Pr substitution led to a slightly lower T_C of 260□. Dielectric measurements for La-[8], and Nd-SBTs[7] revealed that the introduction of V**Erreur!** at the *A* site decreased T_C, as was observed for La-substituted $PbTiO_3$[14]. However, we could not find any relation between T_C and the ionic radius of RE^{3+} for RE-SBTs.

Figure 5 shows the polarization hysteresis loops measured using dense ceramics at 25□. The $2P_r$ and $2E_c$ values at a maximum applied field (E_m) of 200 kV/cm are listed in Table IV. Pr-SBT(x=0.2) exhibited a $2P_r$ of 21 μC/cm^2, which was much larger than that of SBT ($2P_r$ =13 μC/cm^2). Ce-SBT(x=0.2) had a smaller $2P_r$ of 18 μC/cm^2, and a higher $2E_c$ (92 kV/cm) compared with Pr-SBT (61 kV/cm). Figure 6 illustrates $2P_r$ as a function of E_m. Not only the saturation value of $2P_r$ of Pr-SBT was larger, but also Pr-SBT exhibited an excellent polarization property (a larger $2P_r$) in the lower E_m region. At an E_m of 30 kV/cm, although the $2P_r$ of Ce-SBT was almost zero, Pr-SBT indicated a $2P_r$ of 11 μC/cm^2. Furthermore, Pr-SBT showed almost the same saturated $2P_r$ as Bi-modified SBT ($Sr_{0.8}Bi_{2.12}Ta_2O_9$), which has been considered as the most promising candidate material for memory applications, while Bi-SBT exhibited almost zero $2P_r$ at an E_m of 30 kV/cm.[11] These results clearly demonstrate that Pr-SBT has an advantage for a low-voltage-operating ferroelectric-memory material, which has been verified by the investigation of Pr-SBT thin films. [12] It is interesting to note for Ce-SBT(x=0.2) shown in Fig. 5(b) that a hysteresis shift toward positive field, so-called "imprint" was observed, and the hysteresis shape was asymmetric. This behavior is often observed for another ferroelectric thin films,[15] and is closely related to space charge such as oxygen vacancies. [16]

Here, we consider structural distortion and P_s originating in ionic displacements. Compared with the paraelectric tetragonal phase with *I*4/*mmm* symmetry, TaO_6 octahedra in the ferroelectric phase with $A2_1am$ orthorhombic symmetry rotate in the *a*-*b* plane as well as tilt away from the ***c*** axis,[4-6] as depicted in Fig. 2. The tilt angle from the ***c*** axis, which can be estimated from the coordinates of O1 and O2, is defined as α, and the components along the ***a*** and ***b*** axes are referred to as α_x (in the *a*-*c* plane) and α_y (in the *b*-*c* plane), respectively. For SBT, α_x was as small as 0.4 deg, while α_y (7.9 deg) was much larger.[7] In the *a*-*b* plane parallel to the Bi_2O_2 layers, TaO_6 octahedra rotate greatly accompanied by the whole shift of TaO_6 octahedra along the ***a*** axis. The rotation angle (β) estimated from the coordinates of O4 and O5 was 4.3 deg for SBT. [7] Ce- and Pr-SBTs showed almost the same α_x, α_y, and as SBT. These results indicate that the substitution of Ce and Pr did not change the overall structural distortion related to ferroelectricity.

Since glide and mirror planes are present along the ***b*** and ***c*** axes, respectively, the local dipole moments caused by the ionic displacements are cancelled out along the ***b*** and ***c*** axes. Thus, the cooperate displacements occur only along the ***a*** axis, leading to a P_s along the ***a*** axis. Using the formal charge (+2 for Sr, +3 for Ce, Pr and Bi, +5 for Ta, -2 for O), we calculated P_s by the following equation:

$$P_s = \Sigma_i (m_i \times \Delta x_i \times Q_i e) / \Omega, \qquad (2)$$

where m_i is the site multiplicity, Δx_i is the atomic displacement along the **a** axis from the corresponding position in the parent tetragonal ($I4/mmm$) structure, $Q_i e$ is the ionic charge for the ith constituent ion, and Ω is the volume of unit cell. The value of P_s for SBT was estimated to be 16.7 μC/cm^2. [7] Pr-SBT(x=0.2) indicated a slightly smaller P_s of 15.0 μC/cm^2 (see Table IV). The Ce substitution did not change the P_s value (16.5μC/cm^2). These results of P_s are consistent with the tendency of T_C that the ferroelectrics with higher T_C have larger P_s. [17] The P_r observed for Ce-SBT was lower than that of Pr-SBT, whereas Ce -SBT has a lager P_s. It is strongly suggested that the lower P_r is caused by pinning of domain motion due to V**Erreur!**, as was often observed for $Bi_4Ti_3O_{12}$ ceramics [18,19]. Furthermore, the imprint behavior of Ce-SBT is also related to V**Erreur!**. In contrast, Pr-SBT did not show the imprint and domain pinning behaviors in spite of having V **Erreur!**. These suggest the difference in polarization properties is attributed to the distribution of V **Erreur!**. In the perovskite layers, the oxygen site are highly distorted due to the rotation and tilting of TaO_6 octahedra, leading to a low V**Erreur!** mobility. In contrast, O3 in the Bi_2O_2 layers consists of an oxygen layer in the *a-b* plane, and V**Erreur!** at the O3 site is likely to have a relatively high mobility. Although V**Erreur!** was present in the perovskite layers in Pr-SBT, the Bi_2O_2 layers did not have V**Erreur!**. Thus, the influence of V**Erreur!** on the polarization properties of Pr-SBT becomes small. For Ce-SBT having a large amount of V**Erreur!** in the Bi_2O_2 layers, V**Erreur!** at the O3 site easily migrates and assembles near domain walls, giving rise to the domain pinning and imprint behaviors. It is suggested for the SBT system that V**Erreur!** in the Bi_2O_2 layers induces a deterioration of the polarization properties. It has been reported also for $Bi_4Ti_3O_{12}$, another bismuth layered ferroelectric material, that oxygen vacancies could be induced both in the perovskite and Bi_2O_2 layers and they cause fatigue failures.[13] This supports above discussion in the SBT system.

Summary

The crystal structure and polarization properties of Ce- and Pr-modified SBTs were investigated. Neutron powder diffraction and X-ray photoelectron analyses revealed that Ce and Pr were substituted at the Sr site as trivalent cations, and that the charge neutrality is satisfied through the formation of Sr vacancies to compensate the charge difference between RE^{3+} and Sr^{2+}. Polarization measurements using dense ceramics indicated that the substitution of Pr markedly improved P_r at low electric field as well as saturated P_r. In contrast Ce-SBT had a lower P_r, and exhibited a hysteresis shift (imprint behavior). The Rietveld analysis of the neutron diffraction data showed that oxygen vacancies as well as Sr vacancies are present, and oxygen vacancies in the Bi_2O_2 layers were observed only for Ce-SBT. It is suggested that the oxygen vacancies in the Bi_2O_2 layers strongly affect polarization properties and induce the deterioration such as domain pinning and imprint behaviors observed for Ce-modified SBT.

ACKNOWLEDGEMENT

The authors acknowledge financial support by *PRESTO*, Japan Science and Technology Corporation (JST), and thank Dr. Osada (NIMS) for fruitful discussion.

References

1. Araujo, C. A-Paz de, Cuchiaro, J. D., Mcmillan L. D., Scott M. C. & Scott J. F., Fatigue-free ferroelectric capacitors with platinum-electrodes. Nature, 1995, **374** 627-629.
2. Park B. H, Kang B. S., Bu S.D., Noh T. W., Lee J. & Jo W., Lanthanum-substituted bismuth titanate for use in non-volatile memories, Nature, 1999, **401**, 682-684.
3. Kim S. K., Miyayama M. & Yanagida H., Electrical anisotropy and a plausible explanation for dielectric anomaly of $Bi_4Ti_3O_{12}$ single crystal, Materials Research Bulletin, 1996, **31**, 121-131.
4. Rae A. D., Thompson J. G. & Withers, R. L., Structure refinement of commensurately modulated bismuth strontium tantalate, $Bi_2SrTa_2O_9$, Acta Crystallographica Sec. B, 1992, **48**, 418-428.
5. Shimakawa Y., Kubo Y., Nakagawa Y., Kamiyama T., Asano H. & Izumi F., Crystal structures and ferroelectric properties of $SrBi_2Ta_2O_9$ and $Sr_{0.8}Bi_{2.2}Ta_2O_9$, Appl. Phys. Lett., 1999, **74**, 1904-1906.
6. Noguchi Y., Miyayama M. & Kudo T., Direct evidence of A-site-deficient strontium bismuth tantalate and its enhanced ferroelectric properties, 2001, **63**, 214102.
7. Noguchi Y., Miyayama M., Oikawa K., Kamiyama T., Osada M. & Kakihana M., Defect engineering for control of polarization properties in $SrBi_2Ta_2O_9$, Jpn. J. Appl. Phys., 2002, 41, 7062-7075.
8. Noguchi Y. & Miyayama M., Cation-vacancy-induced low coercive field in La-modified $SrBi_2Ta_2O_9$, J. Appl. Phys. 2004, **95**, 4261–4266.
9. Kamiyama, T., Oikawa, K., Tsuchiya, N., Osawa, M., Asano, H., Watanabe, N., Furusawa, M., Satoh, S., Fujikawa, I., Ishigaki, T. & Izumi, F., Physica B, 1995, **213-214**, 875-877.
10. Ohta, T., Izumi, F., Oikawa, K. & T. Kamiyama, Rietveld analysis of intensity data taken on the TOF neutron powder diffractometer VEGA, Physica B, 1997, **234**, 1093-1095.
11. Noguchi Y., Kitamura A., Woo L. C., Miyayama M., Oikawa K. & Kamiyama T., Praseodymium-modified $SrBi_2Ta_2O_9$ with improved polarization properties at low electric field, J. Appl. Phys., 2003, **94**, 6749-6752.
12. Kitamura A., Noguchi Y. & Miyayama M., Polarization properties of praseodymium-modified $SrBi_2Ta_2O_9$ ceramics and thin films prepared by sol–gel method, Mater. Lett., 2004, **58**, 1815-1818.
13. Park, B. H., Hyun, S. J., Bu, S. D., Noh, T. W., Lee, J., Kim, H.-D., Kim, T. H. & Jo W., Differences in nature of defects between $SrBi_2Ta_2O_9$ and $Bi_4Ti_3O_{12}$, Appl. Phys. Lett., 1999, **74**, 1907-1909.
14. Kim T.-Y. & Jang H. M., B-site vacancy as the origin of spontaneous normal-to-relaxor ferroelectric transitions in La-modified $PbTiO_3$, Appl. Phys. Lett.,2000, 77, 3824-3826.
15. Lee. J. & Ramesh R., Imprint of $(Pb,La)(Zr,Ti)O_3$ thin films with various crystalline qualities, Appl. Phys. Lett. 1996, **68**, 484-486.
16. Friessnegg, T., Aggarwal, S., Ramesh, R., Nielsen, B., Poindexter, E. H. & Keeble D. J., Vacancy formation in $(Pb,La)(Zr,Ti)O_3$ capacitors with oxygen deficiency and the effect on voltage offset, Appl. Phys. Lett. 2000, **77**, 127-129.
17. Irie, H., Miyayama, M. & Kudo T., Structure dependence of ferroelectric properties of bismuth layer-structured ferroelectric single crystals, J. Appl. Phys., 2001, **90**, 4089-4094.
18. Noguchi Y., Miwa I., Goshima Y. & Miyayama M., Defect control for large remanent polarization in bismuth titanate ferroelectrics, doping effect of higher-valent cations, Jpn. J. Appl. Phys., 2000, **39**, L1259-L1262.
19. Noguchi Y. & Miyayama M., Large remanent polarization of vanadium-doped $Bi_4Ti_3O_{12}$, Appl. Phys. Lett., 2001 **78**, 1903-1905.

Table I *R* factors and refined lattice parameters.

Samples	R_{wp} (%)	S(=R_{wp}/R_e)	*a* (nm)	*b* (nm)	*c* (nm)	*V* (nm^3)
SBT [a]	5.74	1.11	0.552 30(2)	0.552 44(2)	2.503 66(4)	0.763 89(4)
Ce-SBT(*x*=0.2)	4.87	1.70	0.551 78(1)	0.551 96(1)	2.501 29(3)	0.761 79(3)
Pr-SBT(*x*=0.2)	4.02	1.35	0.551 72(2)	0.551 89(2)	2.501 53(5)	0.761 69(3)

[a] Ref. 7.

Table II. Structural refinement results for $Ce_{0.13}Sr_{0.8}Bi_2Ta_2O_9$($x$=0.2) at 25□ Žspace group $A2_1am$. Numbers in parentheses indicate standard deviations of the last significant digits.

Atoms	Position	x	y	z	Occupancy	B_{eq}□ 1$0^{-2}$ (nm^2)
Sr/Pr	4*a*	0	0.255 85(75)	0	0.8/0.133	0.44 (4)
Bi	8*b*	0.467 12 (77)	0.771 74 (44)	0.200 42 (5)	1	1.37 (5)
Ta	8*b*	0.514 2 (10)	0.748 59 (59)	0.414 99 (5)	1	0.27 (3)
O(1)	4*a*	0.528 3 (12)	0.293 1 (10)	0	0.967(9)	0.56 (9)
O(2)	8*b*	0.523 1 (11)	0.692 13 (66)	0.341 47 (8)	1.00(1)	1.10 (6)
O(3)	8*b*	0.739 0 (11)	0.993 31 (63)	0.250 36 (12)	0.983(6)	0.46 (5)
O(4)	8*b*	0.755 0 (12)	0.982 60 (70)	0.069 27 (8)	0.990(9)	0.51 (6)
O(5)	8*b*	0.793 7 (11)	0.977 44 (69)	0.583 55 (9)	1.00(1)	0.72 (6)

Table III. Structural refinement results for $Pr_{0.13}Sr_{0.8}Bi_2Ta_2O_9$($x$=0.2) at 25□ Žspace group $A2_1am$. Numbers in parentheses indicate standard deviations of the last significant digits.

Atoms	Position	x	y	z	Occupancy	B_{eq}□ 1□$^{-2}$ (nm^2)
Sr/Pr	4*a*	0	0.253 05(63)	0	0.8/0.133	0.50 (4)
Bi	8*b*	0.467 64 (68)	0.772 82 (37)	0.200 30 (4)	1	1.42 (4)
Ta	8*b*	0.511 97 (92)	0.747 95 (51)	0.414 96 (4)	1	0.21 (2)
O(1)	4*a*	0.525 3 (11)	0.295 24(85)	0	0.961(7)	0.52 (8)
O(2)	8*b*	0.520 17 (94)	0.693 85 (58)	0.341 71 (7)	1.00(1)	1.18 (5)
O(3)	8*b*	0.736 5 (10)	0.994 03 (52)	0.250 57 (10)	1.00(1)	0.55 (3)
O(4)	8*b*	0.751 7 (11)	0.983 81 (62)	0.069 06 (7)	0.983(7)	0.52 (5)
O(5)	8*b*	0.791 3(10)	0.976 67 (59)	0.583 78 (8)	0.988 (7)	0.72 (6)

Table IV Polarization properties and Spontaneous polarization (P_s) estimated from the structural data

Samples	$2P_r$ (μC/cm^2) [a]	$2E_c$ (kV/cm) [a]	P_s (μC/cm^2) [b]	α_x (deg)	α_y (deg)	β (deg)
SBT [c]	13	57	16.7	0.4	7.9	4.3
Ce-SBT(x=0.2)	18	92	16.5	0.4	8.0	4.4
Pr-SBT(x=0.2)	21	61	15.0	0.4	8.0	4.5

[a] At the applied field of around 200 kV/cm.

[b] Calculated using the formal charges (see text).

[b] Ref. 7.

Figure Captions

Fig. 1 Results of the Rietveld analysis for neutron powder diffraction of (a) $Ce_{2x/3}Sr_{1-x}Bi_2Ta_2O_9$ [Ce-SBT (x=0.2)] and (b) $Pr_{2x/3}Sr_{1-x}Bi_2Ta_2O_9$ [Pr-SBT (x=0.2)]. Δ indicates the difference between calculated and observed values.

Fig.2 Schematic representations of TaO_6 octahedral revolution in perovskite blocks: (a) tilt from the c axis (the component along the **a** axis is referred to as α_x) and (b) average rotation in the a□b plane (angle β). O(1) and O(2) are apex oxygen atoms. O(1) is shared by two TaO_6 octahedra, while O(2) bonds to the Bi in Bi_2O_2 layers. The Bi_2O_2 layers contain a plane composed of O(3). Dashed circles show the oxygen atoms in a paraelectric state.

Fig.3 Lattice parameters and volume (V) as a function of the ionic radius at the 12-coordinated site of RE^{3+}.

Fig.4 Temperature dependence of dielectric permittivity of dense ceramics.

Fig.5 Polarization properties measured using dense ceramics at 25□ for Ce-SBT(x=0.2) and Pr-SBT(x=0.2).

Fig. 6 Maximum applied field (E_m) dependence of $2P_r$ for Ce-SBT(x=0.2) and Pr-SBT(x=0.2)

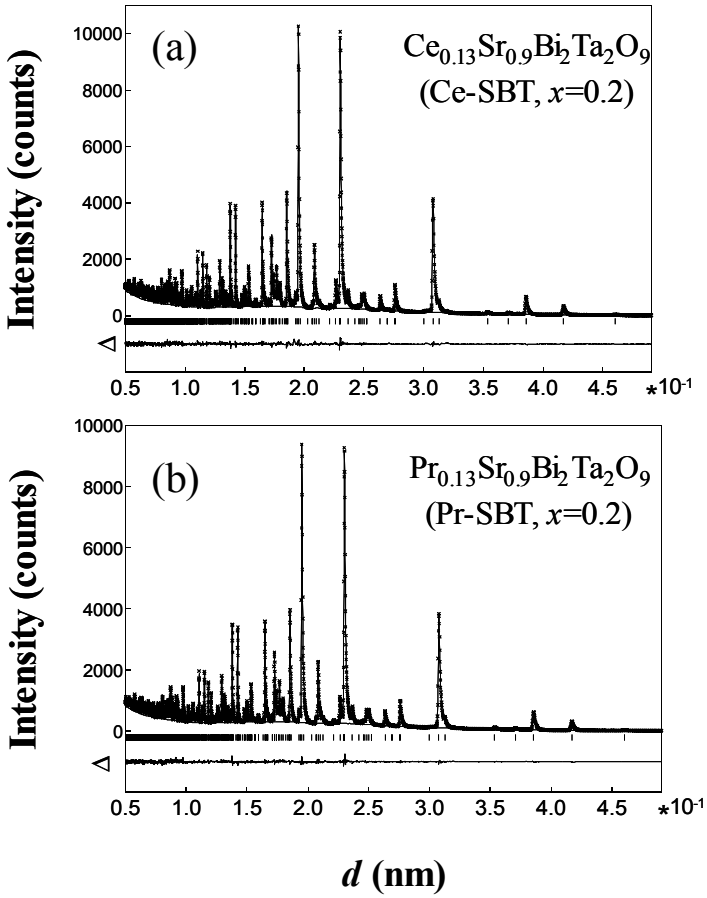
(a)
$Ce_{0.13}Sr_{0.9}Bi_2Ta_2O_9$
(Ce-SBT, x=0.2)
(b)
$Pr_{0.13}Sr_{0.9}Bi_2Ta_2O_9$
(Pr-SBT, x=0.2)
Intensity (counts)
Intensity (counts)
10000
8000
6000
4000
2000
0
Δ
0.5 1.0 1.5 2.0 2.5 3.0 3.5 4.0 4.5 *10-1
d (nm)

Fig. 1

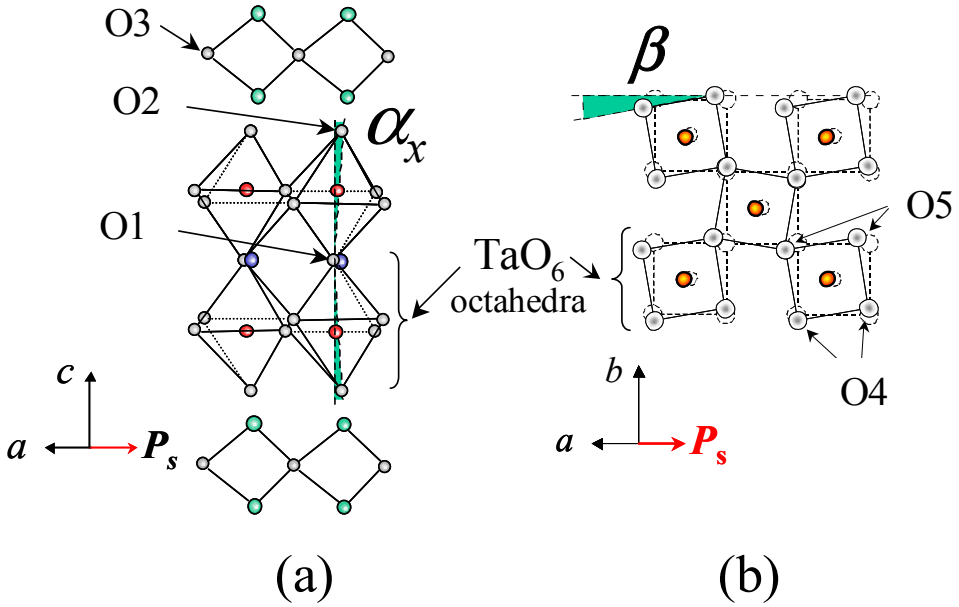

Fig. 2

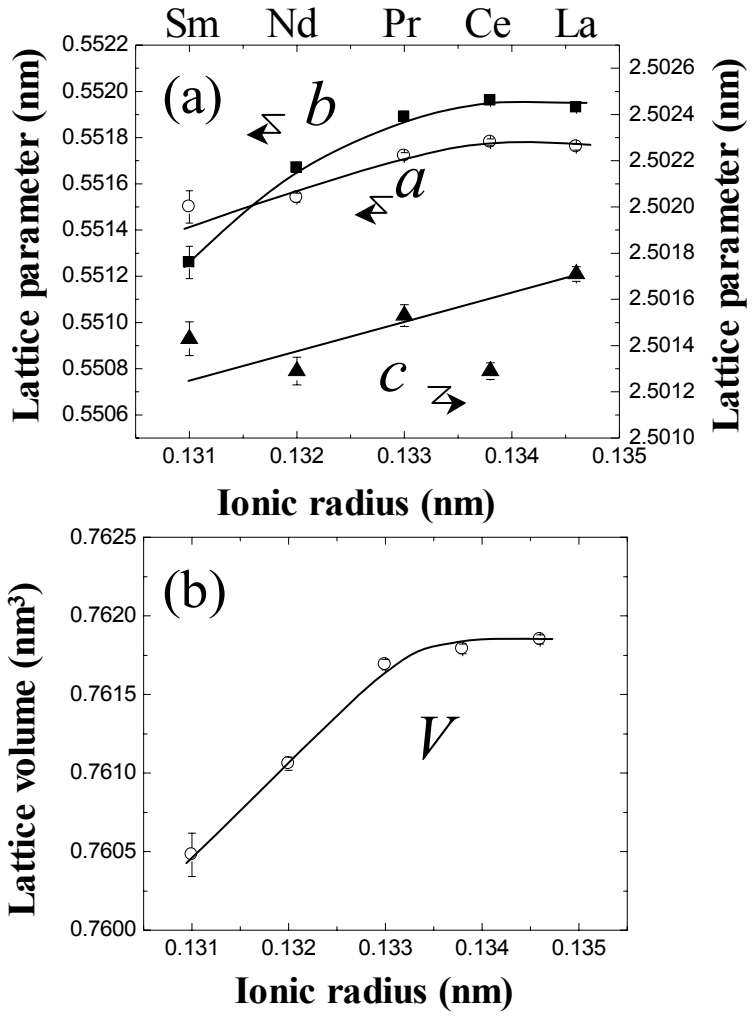
Sm
Nd
Pr
Ce
La
(a)
b
a
c
Lattice parameter (nm)
Lattice parameter (nm)
0.5522
0.5520
0.5518
0.5516
0.5514
0.5512
0.5510
0.5508
0.5506
2.5026
2.5024
2.5022
2.5020
2.5018
2.5016
2.5014
2.5012
2.5010
0.131
0.132
0.133
0.134
0.135
Ionic radius (nm)
(b)
V
Lattice volume (nm3)
0.7625
0.7620
0.7615
0.7610
0.7605
0.7600
0.131
0.132
0.133
0.134
0.135
Ionic radius (nm)

Fig. 3

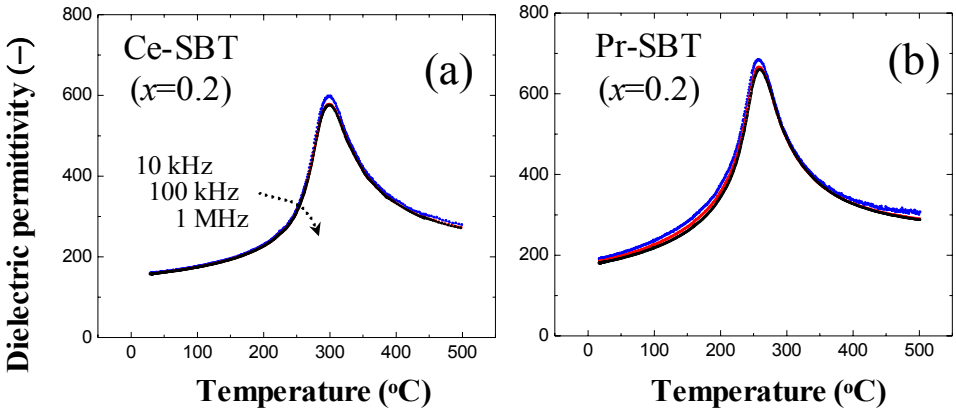
Dielectric permittivity (–)
800
600
400
200
0
Ce-SBT
(x=0.2)
(a)
10 kHz
100 kHz
1 MHz
0
100
200
300
400
500
Temperature (°C)
Pr-SBT
(x=0.2)
(b)
Temperature (°C)

Fig. 4

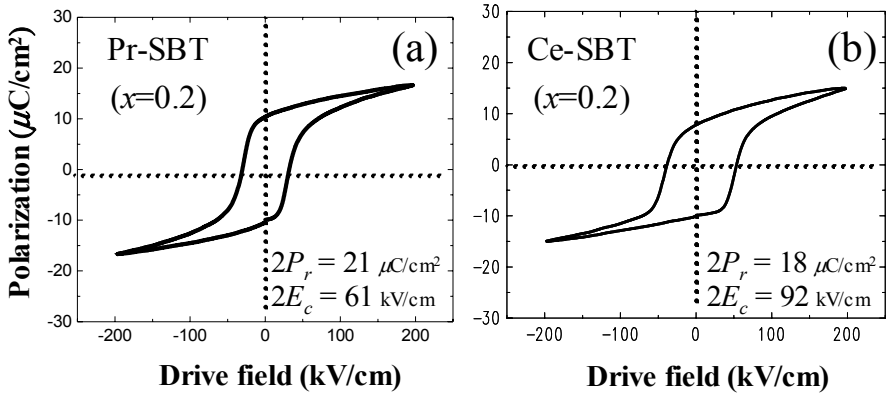
Pr-SBT
(x=0.2)
(a)
2Pr = 21 μC/cm²
2Ec = 61 kV/cm
Polarization (μC/cm²)
Drive field (kV/cm)
Ce-SBT
(x=0.2)
(b)
2Pr = 18 μC/cm²
2Ec = 92 kV/cm
Drive field (kV/cm)

Fig. 5

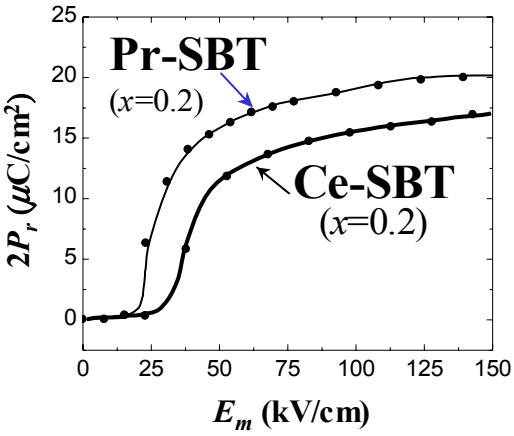
Pr-SBT
(x=0.2)
Ce-SBT
(x=0.2)
2Pr (μC/cm²)
Em (kV/cm)
0
5
10
15
20
25
0
25
50
75
100
125
150

Fig. 6